Two-dimensional imaging of two types of radicals by the CW-EPR method

Tomasz Czechowski [a,*], Ryszard Krzyminiewski [a], Jan Jurga [b], Wojciech Chlewicki [c]

[a] *Medical Physics Department, Institute of Physics, Adam Mickiewicz University, Umultowska 85, 61-614 Poznan, Poland*
[b] *Institute of Materials Technology, Poznan University of Technology, Poznan, Poland*
[c] *Institute of Electronics, Telecommunication and Computer Science, Technical University of Szczecin, Poland*

Abstract

The CW-EPR method of image reconstruction is based on sample rotation in a magnetic field with a constant gradient (50 G/cm). In order to obtain a projection (radical density distribution) along a given direction, the EPR spectra are recorded with and without the gradient. Deconvolution, then gives the distribution of the spin density. Projection at 36 different angles gives the information that is necessary for reconstruction of the radical distribution. The problem becomes more complex when there are at least two types of radicals in the sample, because the deconvolution procedure does not give satisfactory results. We propose a method to calculate the projections for each radical, based on iterative procedures. The images of density distribution for each radical obtained by our procedure have proved that the method of deconvolution, in combination with iterative fitting, provides correct results. The test was performed on a sample of polymer PPS Br 111 (*p*-phenylene sulphide) with glass fibres and minerals. The results indicated a heterogeneous distribution of radicals in the sample volume. The images obtained were in agreement with the known shape of the sample.
© 2007 Elsevier Inc. All rights reserved.

Keywords: Electron Paramagnetic Resonance Imaging; Radicals; Imaging; Deconvolution; Reconstruction; SART

1. Introduction

In Electron Paramagnetic Resonance Imaging (EPRI) deconvolution has been used to determine spatial profiles or projections for samples with one paramagnetic species and constant lineshape. The accuracy of the resulting images depends on the signal to noise ratio of the input experimental data and on the type of the deconvolution technique applied. The deconvolution can be done by Fourier transformation, iteratively or algebraically. The deconvolution function can be a Gaussian or Lorentzian theoretical curves, or an experimental spectrum.

For example, in the Fourier transform method the ratio of the transforms of the EPR spectra recorded in the presence and the absence of the field gradient is calculated and the result is reverse Fourier transformed [1,3]. The method is fast and simple but it does not give satisfactory results because of increased noise that arises from noisy data and division by values close to zero. Spatial profiles for a reference sample, obtained by Fourier deconvolution, without filtering, had a S/N ratio of about 3, although the S/N for spectra recorded in the presence of the field gradient was about 30. Addition of a filter function and/or the use of a theoretical spectrum (either a Gaussian or a Lorentzian) as the deconvolution function should improve the results [2]. This procedure can be successfully applied when the EPR spectrum of the radical to be imaged has no hyperfine structure.

Another method for improving the quality of the density distributions is based on zeroing the high frequency components of the Fourier transforms of the EPR spectra recorded in the presence and in the absence of the field gradient [1], or multiplication of the ratio of the Fourier transforms by a Hamming [4], logarithmic [5] or other filter function [6].

* Corresponding author. Fax: +48 61 8295758.
E-mail address: tomczech@interia.pl (T. Czechowski).

A very interesting possibility is Fourier reconstruction [10]. In this method the images are obtained without the need for Filtered Back Projection (FBP). As in other Fourier methods, the quality of the images obtained without appropriate filters is not satisfactory.

Another approach to obtaining images $y(n)$ is the algebraic method [7] in which:

$$y(n) = x(n)/H(n,n) \qquad (1)$$

where $x(n)$ is the recorded EPR spectrum at a given angle with respect to the gradient direction, while $H(n,n)$ is the filtering matrix made on the basis of the EPR spectrum recorded without the gradient. The choice of the filtering matrix $H(n,n)$ determines the distribution of a given type of radicals along a selected direction and it affects the resolution of the reconstructed images.

$$H(n,n) = \begin{bmatrix} h(1) & 0 & 0 & \cdots & 0 \\ h(2) & h(1) & 0 & & \\ h(3) & h(2) & h(1) & & \\ \vdots & & & & \vdots \end{bmatrix} \qquad (2)$$

where $h(m)$ is a part of the $g(n)$ spectrum that is the EPR spectrum with no gradient applied. The optimum choice of the matrix $H(n,n)$ depends on the choice of $h(m)$:

$$\sum_{i=1}^{m} h(i) = \sum_{i=1}^{b-a} g(i+a) \qquad (3)$$

The parameters a, b and m are interrelated by $m = b - a$. The parameters a and b define cutoffs for significant intensity at the beginning and end of the lineshape. The choice of the parameters a and b determines the quality of the $y(n)$ projections obtained [14]. This method permits getting the projections from EPR spectra with hyperfine structure or those characterised by a low S/N ratio (<30). The algebraic method of getting the projections has been reviewed in [8,11,12]. The method permits obtaining two-dimensional distributions of a given radical and when applied together with advanced filtering techniques it permits obtaining distributions with improved S/N ratio [9].

Iterative methods are the most time-consuming but they offer the possibility to obtain projections for distributions of one or two different type radicals. The methods provide very good quality because, unlike the algebraic method, the whole spectrum is analysed. Therefore, the resolution of the images is increased and the effect of broadening of the distributions is reduced.

In the following we present the results obtained by the iteration method applied to one or two types of radicals.

2. Apparatus

The 2D images were obtained by the CW method on a Bruker X-band EMX spectrometer, with gradient coils and a goniometer [14]. The gradient coils are 230×13 mm, made of copper wire of 1 mm in diameter.

The field gradient constant is 27 G/cm A and the maximum current that can be applied for prolonged periods is 2 A. A field gradient of 80 G/cm can be generated for up to 1 min for a current of 3 A. The maximum sample size is 9 mm. The data are collected as a function of sample orientation with and without a gradient. The number of orientations should be as high as possible to get good quality image.

3. 1D deconvolution

The iterative analysis proceeds as follows:

- For a selected orientation of the sample with respect to the external magnetic field the EPR measurements are performed with $x(n)$ and without $g(n)$ a gradient. It should be noted that the range of the scanned magnetic field and other parameters of measurements must be the same.
- We look for the minimum of the following expression:

$$b_{j,l}^{(k)} = \sum_{i=1}^{n} |(x(i) - x1(i)_{j,l}^{(k)})|$$
$$l = -10, -9, \ldots, 9, 10 \quad j = 1, 2, \ldots, n-m+1 \qquad (4)$$

where $x(n)$ is the EPR spectrum recorded with gradient and $x1(n)$ is a simulated EPR spectrum obtained as a result of convolution of the linear distribution of the radical $y(n-m+1)$ and spectrum $h(m)$ (Eq. (3)), the region of the spectrum in the absence of gradient that defines all spectral features. The parameter j is the index within the linear distribution of the radical $y(n-m+1)$, l describes how many steps will be used to change each element of $y(n-m+1)$, and k is the number of the iteration. The simulated spectrum $x1(n)$ is obtained by a convolution for the following data:

$$x1_{j,l}^{(k)} = h(m) \times y(j)_l^{(k)} \qquad (5)$$

The method of iterative fitting is based on subsequent changes in each of the simulated parameters $y(j)$ in such a way as to minimise the discrepancy (Eq. (4)). For the parameters $y(j)$ the following procedure is used:

$$y(j)_l^{(k)} = y(j)^{(k-1)}(1 + p \cdot l) \qquad (6)$$

where p is the iteration step in the range 0.25–1% of maximum value. At first $y(j)$ is adjusted so that the calculated change in the spectrum $x1(n)$ would reduce the error (Eq. (4)). The procedure involves changes in $y(i)$ within 10% of its value with a step p. At the beginning of the calculations it is advisable to choose a larger step to shorten the calculation time. At the final stage of the calculations the changes in $y(i)$ should be small to get a more accurate fit of $x1(n)$ to $x(n)$ and hence a more accurate distribution $y(n-m+1)$. The choice of a new $y(j)^{(k)}$ is made for l, which the error $b_{j,l}^{(k)}$ is smallest. This cycle is repeated for
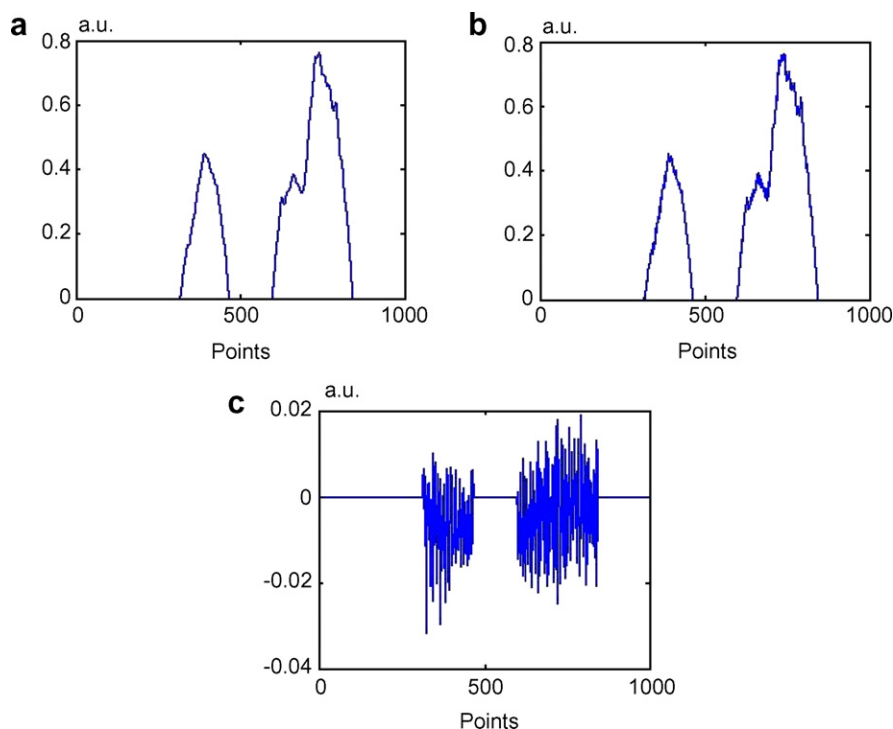
Fig. 1. A certain theoretical density distribution of the radical characterised by a single EPR line was assumed (b), result of 1D deconvolution (a) and difference between theoretical and simulated distribution (c).

all $y(j)$, then it is restarted with the new values of the distribution $y(n - m + 1)$. As a result the simulated distribution of the radical density $y(n - m + 1)$ becomes increasingly close to its actual distribution.

The accuracy of the results obtained by the iteration procedure was tested. A certain theoretical density distribution of the radical characterised by a single EPR line was assumed (Fig. 1b) and then the EPR $x(n)$ spectra were simulated and treated as experimental data in further analysis. The 1D deconvolution was used to calculate the density distribution from the simulated $x(n)$ spectra (Fig. 1a). The agreement between the calculated and assumed projection proves that the iterative method was applied correct.

The error in the generation of a projection is within 1%, which indicates that this method can be applied to experimental spectra (Fig. 1c).

The next aim of our study was to verify the effectiveness of the above-described method for generation of a known distribution. The verification was made on the previously reported EPR data for three samples of DPPH placed in three holes with 1 mm diameter separated by 3 mm [14]. The depth of one of the holes was twice than that of the other two, so the signal should be twice as large. The iterative method called simultaneous algebraic reconstruction technique (SART) proposed by Kak [17,18] was used. The images obtained by the SART method are constructed
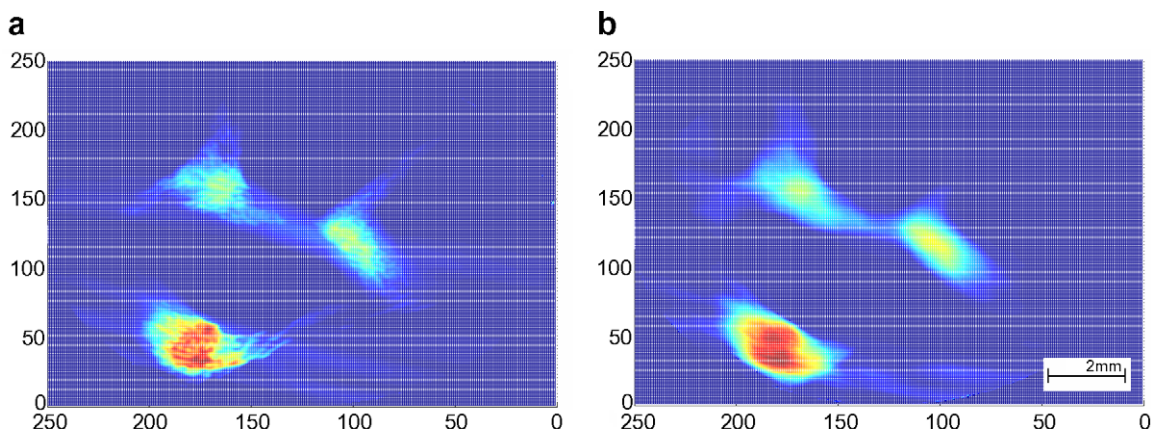

Fig. 2. Distribution for three samples of DPPH placed in three holes with 1 mm diameter separated by 3 mm [14] obtained by two deconvolution techniques: (a) iterative, (b) algebraic (golden deconvolution).

on the basis of the radical density distribution function $Y(n)$ determined for each projection.

The reconstructed image corresponded well with the known distribution of the DPPH radical. The method can be directly compared with the procedure that was used previously [14], which was based on the so-called golden deconvolution (Eq. (1)), also known as algebraic deconvolution. The image obtained by iterative deconvolution (Fig. 2a) showed much more details than that obtained on the basis of the golden deconvolution (Fig. 2b). The success of the method of iterative deconvolution prompted us to propose an analogous method that could be applied to generate images of two different types radicals present in one sample.

4. 2D deconvolution

Iterative deconvolution of the image of two types of radicals is much more complicated then for one type radical. In order to obtain the distribution of the radical along a given direction, the EPR spectrum $g(n)$ has to be first recorded without gradient, to find the shape and structure of the EPR line of a given radical. The EPR lines of two radicals may overlap. If this is so, the spectrum must be separated into the contributions from the two radicals. Next, for a selected orientation, the EPR spectrum $x(n)$ is recorded with magnetic gradient. We look for the minimum of fit error $b_{j,l1,l2}^{(k)}$ (Eq. (4)). The simulated spectrum $x1(n)$ of the two types radicals can be expressed as

$$x1_{j,l1,l2}^{(k)} = h(m) \times y1(j)_{l1}^{(k)} + k(p) \times y2(j)_{l2}^{(k)}$$
$$l1, l2 = -10, -9, ..., 9, 10 \qquad (7)$$

where the $h(m)$ and $k(p)$ files contain the information on the shape of the EPR line of the first and the second type radical, respectively, $y1(n - m + 1)$ and $y2(n - p + 1)$ are the linear distributions of the first and the second type radical along a given direction, respectively. The fitting procedure of $x1(n)$ to $x(n)$ is made by small changes in the parameters of the former leading to minimisation of the fit error $b_{j,l1,l2}^{(k)}$ (Eq. (4)). The changes are made by iterative fit of each of the parameters $y1(j)$ and $y2(j)$. For the two distributions at the jth point the following steps are made.

$$yi(j)_{il}^{(k)} = yi(j)^{(k-1)}(1 + p \cdot l)i \quad \text{where } i = 1, 2 \qquad (8)$$

The choice of a new $y1(j)^{(k)}$ and $y2(j)^{(k)}$ is made for $l1$ and $l2$, such that the error $b_{j,l1,l2}^{(k)}$ is minimised. This cycle is repeated for all j, then it is restarted with the new values of the distribution $y1(n - m + 1)$ and $y2(n - p + 1)$.

The proposed procedure has been tested on the theoretical distributions of radical density. We assumed that the sample studied contains two types of radicals characterised
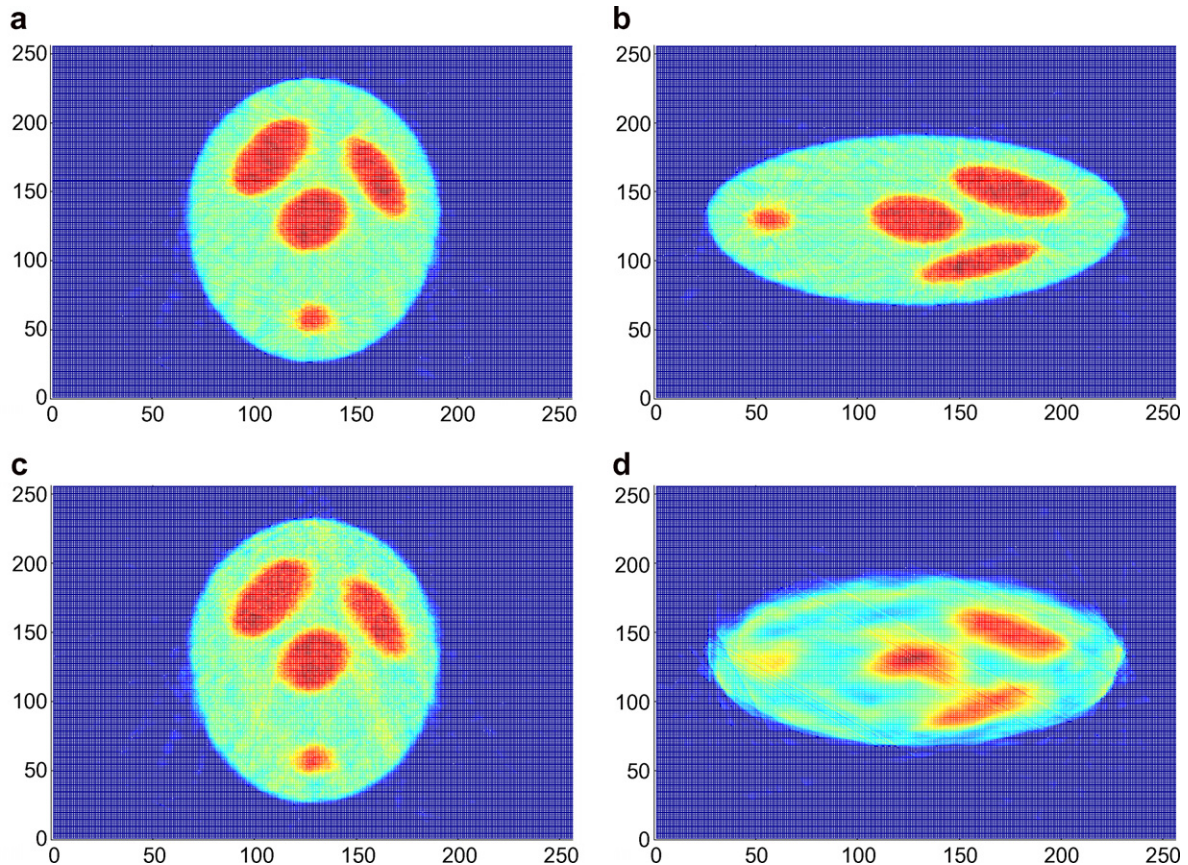

Fig. 3. Result for two types of radicals reconstructed using theoretical projections for (a) radical with a single narrow line, and (b) radical with a five-line EPR signal, and using iterative projections (c) and (d). All images were reconstructed by the SART method used 18 projections.

by different EPR lines: one by a single and narrow line, while the other by five EPR lines. The distribution of the radicals was also assumed to differ significantly. By iterative deconvolution we obtained projections for each type radical. We used 18 theoretical spectra $x(n)$ to define 18 different projections. The images were reconstructed by the SART method. The density distribution of the radical characterised by the single EPR line was very well reproduced with an error smaller than 1% (Fig. 3c). The only differences between expected projection and ones obtained

using the 2D iterative deconvolution were high frequency components, which is similar to what was observed for 1D images (Fig. 1c). The reproduction of the distribution of the second radical density was much poorer (Fig. 3d). The error of the projection fit reached 5% and the images were noisier because for more complicated radical lines each projection had not only high frequency but also low frequency projection error. In addition, the concentration of the radical with the single line spectrum was four times larger than for the radical with the five-line spectrum.
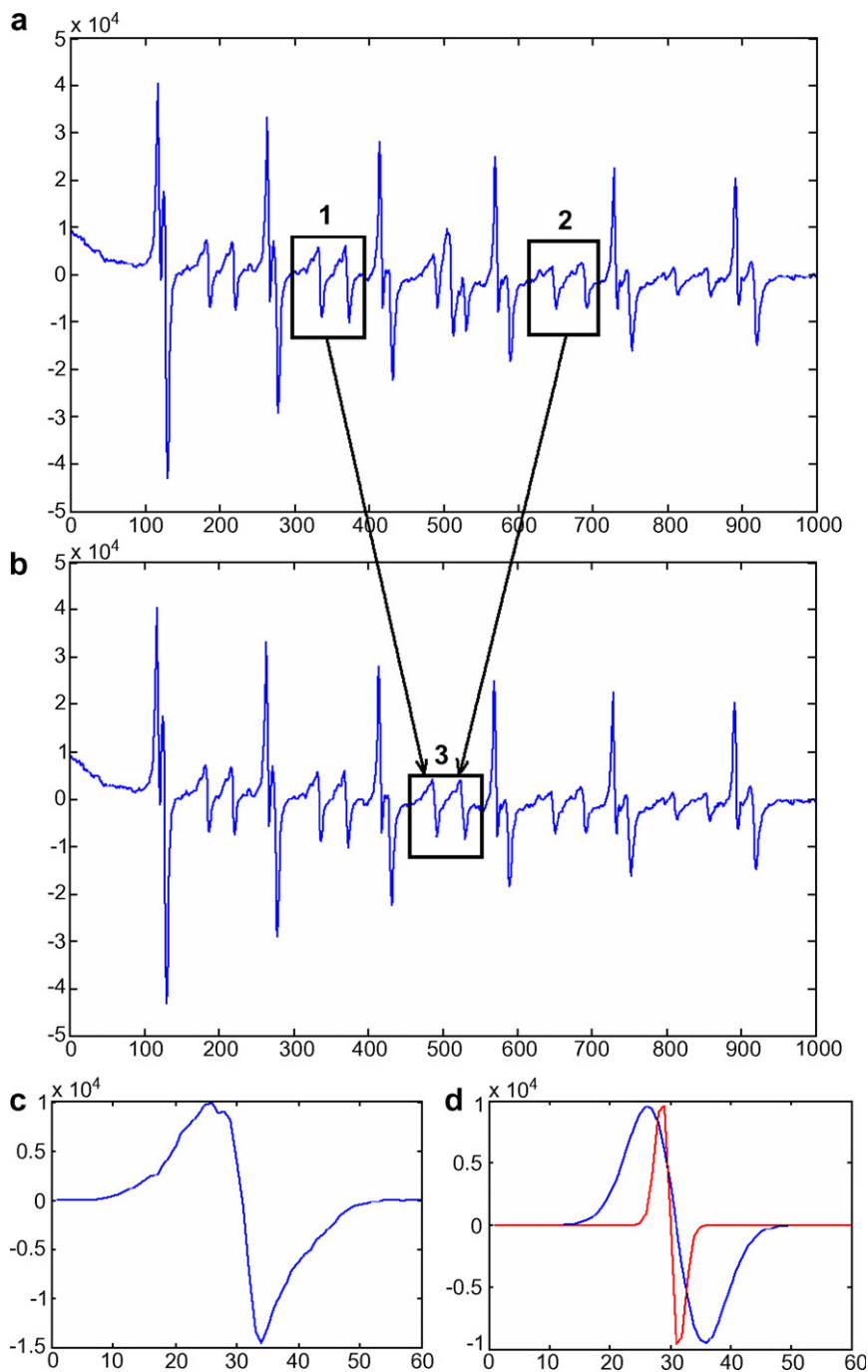

Fig. 4. EPR spectrum of polymer PPS Br 111 sample: Experimental (a), manganese Mn^{2+} EPR spectrum (b) founded using average information about EPR line from boxes 1 to 2, difference between manganese Mn^{2+} EPR spectrum and experimental spectrum (c), components of the radical spectrum (d).

Therefore, for Fig. 3b and d the density distribution was scaled up by a factor of four to clearly show all errors. Big distortion this type of radical distribution (Fig. 3d) compare witch single line radical (Fig. 3c) was mostly come from differences between $h(m)$ and $k(p)$ files contain the information on the shape of the EPR line of the first and the second type radical. Parameter p was approximately five times longer than parameter m, and this was major reason why projection fit error was bigger for five-line radical. Apart from the iterative method, other methods have been proposed for obtaining the distribution of densities of more than one radical [13,15,16].

5. Test on polymer

The method for determination of the density distribution of radicals was tested on polymer PPS Br 111 (*p*-phenylene sulphide) containing 63% cross-linked glass fibre and mineral fillers. The EPR spectrum recorded without gradient shows the signal from a radical (around $x = 500$) in addition to the characteristic lines assigned to Mn^{2+}. To reconstruct images of all types of radicals in the sample, they should be first separated and assigned to particular radicals. This procedure is not trivial as the lines overlap (Fig. 4). The following procedure was proposed. The spectrum in the absence of the gradient was recorded. The intensity and structure of the

EPR lines at lower magnetic field than the radical area (region 1) and at higher magnetic field (region 2) are assumed to correspond to the spectrum of pure manganese Mn^{2+} (Fig. 4a). The average of the signals in these two ranges was used as an estimate of the Mn^{2+} spectrum in region 3 (Fig. 4b). The spectrum of the radicals (Fig. 4c) was calculated by subtracting the spectrum in Fig. 4b from the experimental non-gradient signal. The difference signal shows that there are at least two radicals in the sample (Fig. 4d) with linewidths of 6 and 0.8 G, respectively. There are large uncertainties in the difference spectrum (Fig. 4d), but this error does not have a large impact on the reconstruction of the distribution of the radicals.

Having determined the EPR spectra of each radical, we can start the procedure of constructing the projections. As follows from the spectrum, the sample contains at least 3 types of paramagnetic centre so the procedure was modified as follows:

- The method of iterative 1D deconvolution was applied to the EPR spectrum of Mn^{2+} ions, the information on the EPR line structure of manganese is included in the $h(m)$ file.
- Having obtained the concentration distribution projection of Mn^{2+}, for a certain angle between the horizontal axis of the sample and the magnetic field gradient we calculate the difference $x(n) - x1(n)$, where x is the EPR spectrum recorded with gradient, $x1$ is the simulated Mn^{2+} spectrum (Eq. (4)) and the result is treated as the EPR spectrum containing information on the radicals in the sample.
- By the iterative 2D deconvolution we get the projections of the two types of radicals (Fig. 4d, Eq. (7)).

A set of 36 projections were recorded at 10° increment. The time of measurement of one projection was 41 s, time constant 41 ms, microwave power 20 mW, sweep width 200 G, length of the spectra 1024, gradient of 50 G/cm. Each projection was accumulated 9 times and the total time of measurement was 4 h.

On the basis of the projections of Mn^{2+} by the method SART we obtained the manganese ion distribution. The
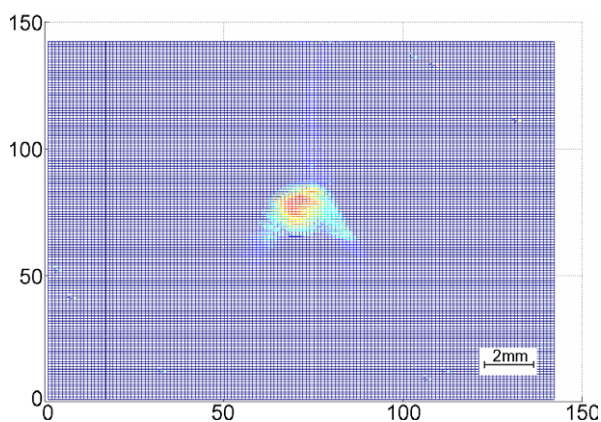

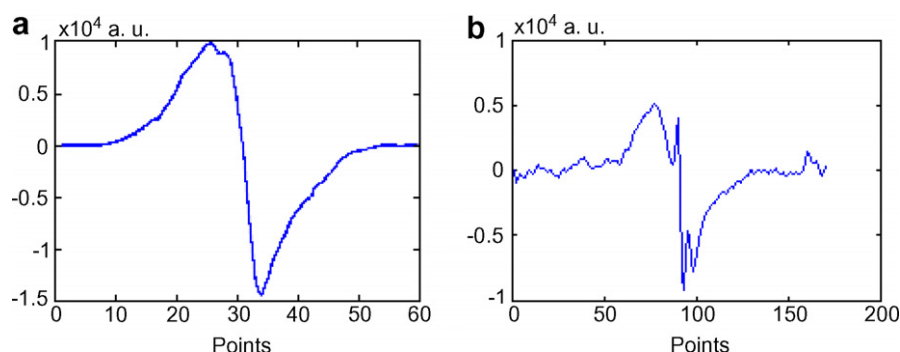Fig. 5. Image of the Mn^{2+} distribution in the samples.

Fig. 6. EPR spectrum of two types of radicals recorded without (a) and with (b) field gradient.

resulting image (Fig. 5) indicates a homogeneous distribution of manganese in sample. The image suggests that the manganese is an impurity in the glass fibre or in the mineral fillers since our previous EPR studies of the polymer PPS did not show any manganese ions [14]. The EPR spectrum of pure glass fibre showed a single line with a width of 6 G, and did not show characteristic Mn^{2+} lines. This excludes the presence of manganese in the glass fibre and supports the supposition that it was introduced with mineral fillers.

The next step was to determine the density distribution of the two types of radicals. To do it we obtained the spectrum containing the information only about these other two types of radicals by subtracting the spectrum of Mn^{2+} contained in the glass fibre from the spectrum recorded with gradient $X(n)$. Therefore, we subtracted from $X(n)$ the spectrum $X1(n)$ obtained by convolution of the EPR spectrum of Mn^{2+} and its projection. Repeating the procedure for each orientation, the EPR $X2(n)$ spectra containing the information on the two types radicals were achieved. The method of iterative deconvolution was applied to get the projections of each type of radical separately. The distribution of the radical with 0.8 G linewidth was insensitive to the magnetic field gradient (Fig. 6). Usually when the magnetic field gradient is applied, the intensity of the EPR line corresponding to a given radical decreases. The larger the gradient, the greater the decrease in the EPR signal intensity. In an extreme case the EPR sig-

nal cannot be detected. Therefore, care must be taken to select a gradient that is small enough to permit detection of the EPR signal. So the EPR line that is insensitive on the magnetic field gradient is not the radical line.

Iron compounds are added to the polymer in the production process. Iron ions can form ferromagnetic cluster giving a single EPR line that is insensitive to the applied gradient. This interpretation can explain the unusual behaviour of the EPR line with 0.8 G width. The image reconstructed in Fig. 7a is not a distribution of the radical density distribution, but together with the spectra presented in Fig. 6, it supports the presence of ferromagnetic Fe^{3+} clusters in the polymer.

Because of the complexity of the spectra, it was difficult to obtain projections of the radical characterised by the EPR line width of 6 G. To minimise the disturbing effect of the spectra of the other types of paramagnetic centres, an additional procedure was applied. The aim of this procedure was a filtration of the shape of the radical density distribution to smooth its contours. No significant effect of the filtering on the error of the fit was noted. To illustrate the effect of filtering on the reconstructed density distribution of the radical characterised by the line width of 6 G, two independent analyses were made with and without filtering. The reconstruction of the density distribution of this radical without an additional filter indicates its cha-
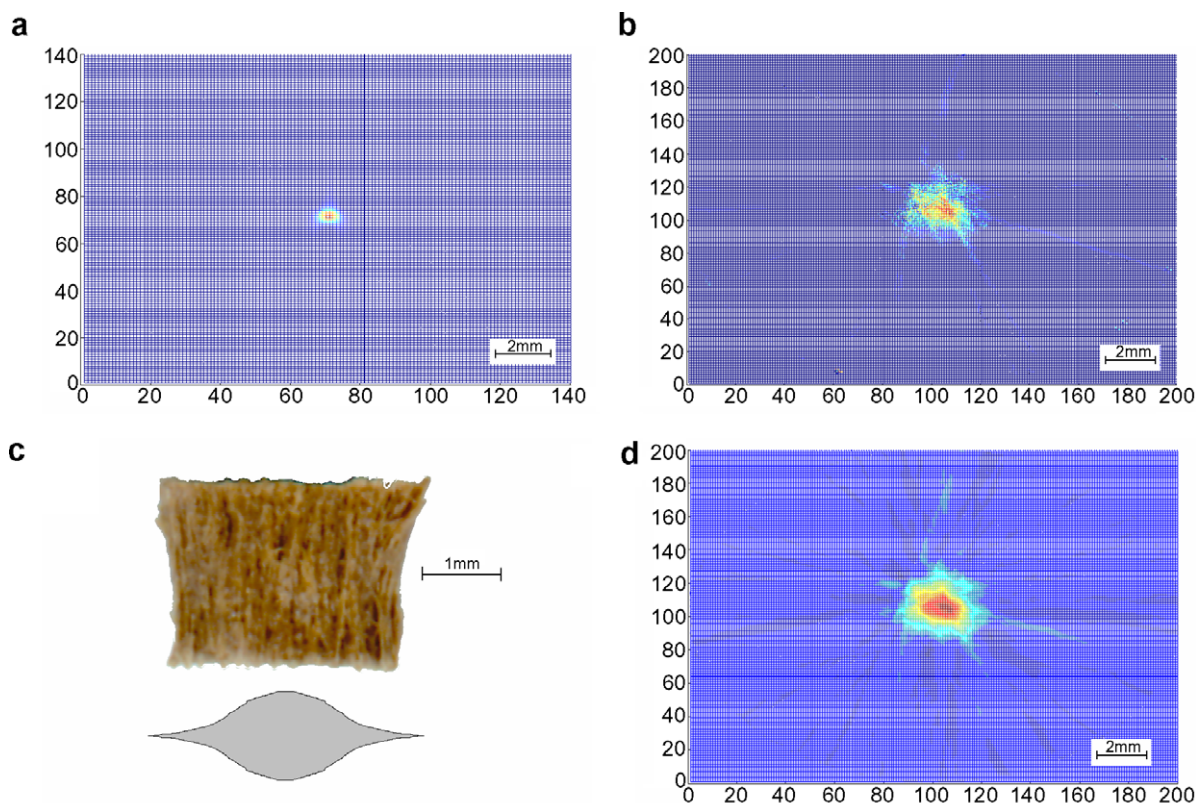

Fig. 7. Distribution of ferromagnetic Fe^{3+} clusters with narrow EPR line (0.8 G width) (a). Distribution of radical with the broad EPR line (6 G width) without (b) and with (d) filtering of projections, both vertical and horizontal shape of the PPS Br 111 polymer sample used for imaging (c).

otic dispersal (Fig. 7b). The images indicated a heterogeneous distribution of the radicals in the sample.

The distribution from Fig. 7b cannot be simply related to the sample shape as show in Fig. 7c. When additional filters were applied, the reconstruction of the 6 G radical density distribution proved its homogeneous presence in the sample (Fig. 7d). The filtering gives the radical density distribution with smoother contours. This distribution corresponds much better to the shape of the polymer sample. To verify which of the radical density distributions is correct, it is necessary to determine the distribution of the radical in the polymer sample. The radical characterised by the EPR line width of 6 G was observed both in the polymer and in the glass fibre sample. In previous investigation of the PPS polymer a homogenous radical distribution has been obtained [14] which is consistent with the proposal of a regular arrangement of the investigated radical in the PPS Br 111 polymer (Fig. 7d). The glass fibre is only 63% cross-linked what make a heterogeneous radical distribution plausible (Fig. 7b). The intensity of the radical signal in the glass fibre is three times higher than in the PPS polymer sample, which supports the suggestion of heterogeneity. The image of the radical distribution obtained without filtering of projections (Fig. 7b), can be interpreted as the distribution of density of glass fibres containing the radical studied. The radical density distribution obtained without filtering is characterised by greater resolution than that obtained with the filtering procedure.

The reconstructions indicate a homogeneous distribution of Mn^{2+} ions in the PPS polymer sample and a chaotic distribution of the radicals characterised by the 6 G EPR linewidth.

6. Conclusions

The proposed method of iterative deconvolution for projections $Y(n)$ of radical distribution from EPR spectrum has been positively verified. This technique permits projections reconstructions with the error below 1% for the EPR spectrum of one type of radical. The reconstructed EPR images of DPPH radical distribution obtained by our procedure have proved that the method of iterative deconvolution provided correct results.

Iterative deconvolution for two different types of radicals in the sample makes it possible to obtain images of the distribution of each radical. Based on the results we can conclude that precision of the reconstruction depends on EPR line structure. Precision of the reconstruction is very good for the radicals characterised by single EPR line and satisfactory for radicals that have more complicated EPR line structure. Worse reconstruction is caused by accumulated errors. It is directly correlated with the size of the data $h(m)$ and $k(p)$ characterising the structure of

radical EPR line. Algorithm of the iterative deconvolution for two types of radicals in the sample did not have any optimisation techniques which help improve radical distribution especially for more complicated EPR line structure. This is our next task to add optimisation techniques inside deconvolution algorithm.

Application of the iterative deconvolution technique allowed an analysis of the radicals distribution in PPS Br 111 polymer sample containing 63% cross-linked glass fibre and mineral fillers. The results indicated a homogeneous distribution of Mn^{2+} ions, and inhomogeneous distribution of free radicals in the sample. The images obtained were in good agreement with the known shape of the sample.

At this stage of the studies the procedure of image reproduction is still very time-consuming (3–4 h) because of a long time needed for measurement of each projection ($\sim$40 s) and the time needed to complete the iterative procedure of image reconstruction (2 h).

References

[1] Y. Deng, G. He, P. Kuppusamy, J.L. Zweier, Magn. Reson. Med. 50 (2003) 444–448.
[2] M. Jonas, E. Marseglia, Radiat. Meas. 27 (1997) 359–363.
[3] K. Ohno, J. Magn. Reson. 50 (1982) 145–150.
[4] G. Placidi, M. Alecci, G. Gualtieri, A. Sotgiu, J. Magn. Reson. A 121 (1996) 60–64.
[5] P.J. Thomas, P.A. Midgley, Ultramicroscopy 88 (2001) 87–194.
[6] H. Busse, K. Wandelt, G.R. Castro, J. Electron Spectrosc. Relat. Phenom. 72 (1995) 311–316.
[7] V.K. Madisetti, D.B. Williams, The Digital Signal Processing Handbook, CRC Press with IEEE Press, 1998, pp. 8-1–8-7.
[8] M. Morháč, J. Kliman, V. Matoušek, M. Veselský, Nucl. Instrum. Methods Phys. Res. A 401 (1997) 385–408.
[9] M. Morháč, V. Matoušek, J. Kliman, Digit. Signal Process. 13 (2003) 144–171.
[10] A.A.M. Maas, P.A.A.M. Somers, Opt. Lasers Eng. 26 (1997) 351–360.
[11] M.M. Morháč, V. Matoušek, J. Kliman, Comput. J. Appl. Math. 140 (2002) 639–658.
[12] P. Bandžuch, M. Morháč, J. Krištiak, Nucl. Instrum. Methods Phys. Res. A 384 (1997) 506–515.
[13] K. Matsumoto, H. Utsumi, Biophys. J. 79 (2000) 3341–3349.
[14] T. Czechowski, R. Krzyminiewski, J. Jurga, W. Chlewicki, Appl. Magn. Reson. 29 (2005) 335–349.
[15] M.M. Maltempo, S.S. Eaton, G.R. Eaton, J. Magn. Reson. 72 (1987) 449–455.
[16] S.S. Eaton, G.R. Eaton, Concept Magnetic Reson. 7 (1995) 49–67.
[17] A.H. Andersen, A.C. Kak, Ultrason. Imaging 6 (1984) 81–94.
[18] A.H. Andersen, IEEE Trans. Med. Imaging 8 (1989) 50–55.